Fast Transmission CT for Determining Attenuation Maps Using a Collimated Line Source, Rotatable Air-Copper-Lead Attenuators and Fan-Beam Collimation

R.J. Jaszczak, D.R. Gilland, M.W. Hanson, S. Jang, K.L. Greer and R.E. Coleman

Department of Radiology, Duke University Medical Center; Department of Biomedical Engineering and Institute of Statistics and Decision Sciences, Duke University, North Carolina

We describe a technique using a line source and a rotatable air-copper-lead assembly to acquire gamma transmission computed tomographic (TCT) data for determining attenuation maps to compensate SPECT emission scans. The technique minimizes problems associated with discriminating ^{99m}Tc transmission and ^{201}Tl emission photons and requires only a modest increase in total study time. A ^{99m}Tc line source and a stacked foil ("multislat") collimator are placed near the focal line of a fan-beam collimator (114 cm focal length) mounted on one detector of a triple-camera SPECT system. We acquired TCT data of plastic rod and anthropomorphic thorax phantoms to investigate the capability of the line source and rotatable air-copper-lead attenuators to determine attenuation maps. The data were acquired with and without 5.4 MBq (145 μCi) of ^{201}Tl placed in the myocardial chamber of the thorax phantom. Phantoms also were scanned using a curved transmission slab source mounted to a parallel-hole collimator. Fan-beam TCT images have improved resolution compared with parallel-beam TCT images. Two patient scans also were performed to evaluate the clinical usefulness of fan-beam TCT. The rotatable air-copper-lead attenuator method eliminates contamination of emission data by transmission photons and reduces spill-over of emission data into the transmission energy window for some cases. Results show the feasibility of using fast, sequential or interlaced transmission scans of a line source within a rotatable air-copper-lead attenuator assembly to obtain accurate attenuation maps for SPECT attenuation compensation.

J Nucl Med 1993; 34:1577–1586

Transmission imaging provides useful additional information for attenuation compensation in single-photon emission computed tomography (SPECT). In the mid-1970s, we designed our first dual-camera SPECT system with the capability to use transmission imaging for body contour determination (*1*). We and other groups have used SPECT systems to acquire gamma ray transmission computed tomographic (TCT) data (*2–10*). Results from previous studies using attenuation information have shown improved image quality with nonuniform attenuation compensation compared with uniform compensation (*3–15*). This improvement motivated us to investigate methods of obtaining attenuation maps using transmission computed tomography. To obtain these maps we designed and built transmission data acquisition systems for a three-headed SPECT camera (Trionix Research Laboratories, Inc., Twinsburg, OH). These systems provide the capability to reconstruct the three-dimensional patient attenuation distribution.

Methods of TCT data acquisition on SPECT cameras are used to acquire transmission and emission data either at separate points in time (sequential scanning) or at the same time (simultaneous scanning). Neither of these methods is ideal and each has unique advantages and problems. Simultaneous acquisition can result in contamination of transmission and/or emission data by improperly detected photons. Sequential transmission/emission acquisition can increase scan time and misregistration of transmission and emission data may present problems. Use of a line transmission source and rotatable air-copper-lead attenuators allows TCT data acquisition before, after or interlaced with the SPECT acquisition. The misregistration problem is alleviated only if TCT acquisition is interlaced, or obtained simultaneously, with the SPECT acquisition. Unless the simultaneous acquisition mode is used, scan time will be increased. In this paper we describe a fast, sequential method for acquiring TCT data.

The primary purpose of this investigation is to show that a line source and rotatable air-copper-lead attenuators are capable of obtaining accurate attenuation maps for nonuniform attenuation compensation in SPECT. The rotatable

Received Nov. 23, 1992; revision accepted May 19, 1993.
For correspondence and reprints contact: Ronald J. Jaszczak, PhD, Dept. of Radiology/Nuclear Medicine, Duke University Medical Center, Box 3949, Durham, NC 27710.

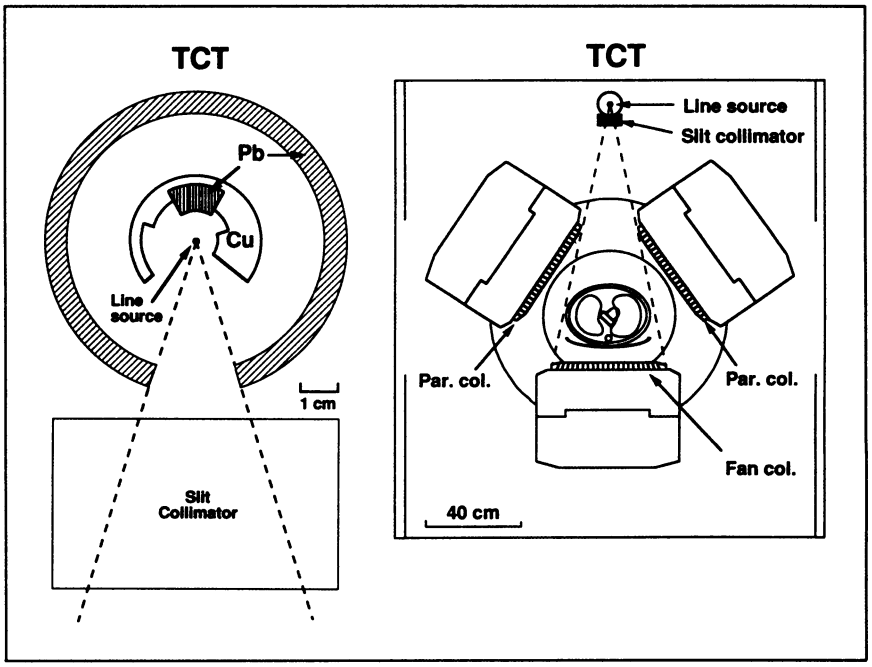

FIGURE 1. Sketch of FB-TCT acquisition system. An enlarged sketch of rotatable air-copper-lead assembly and multislat collimator is shown on the left.

air-copper-lead attenuator method is evaluated using a plastic "cold" rod phantom and an anthropomorphic thorax phantom. Fan-beam (FB) TCT data are acquired using a ^{99m}Tc-filled line source and compared with reconstructed TCT images obtained with parallel-beam TCT. Fan-beam TCT reconstructed images are obtained with and without ^{201}Tl activity in the myocardial chamber of the thorax phantom.

MATERIALS AND METHODS

System Overview

The FB-TCT system has the following major components:

1. A resealable and fillable line source containing an appropriate gamma emitter.
2. A rotatable air-copper-lead attenuator mechanism that allows air, lead or copper to be positioned between the line source and the object being scanned.
3. A stacked multifoil ("multislat") lead collimator that is positioned close to the line source.
4. A long, focal-length fan-beam collimator that is placed on the opposing scintillation camera.
5. The opposing large field-of-view scintillation camera.

The main components are shown in the sketch (Fig. 1) of the FB-TCT system mounted on our triple-camera SPECT scanner.

Line Source and Rotatable Air-Copper-Lead Attenuator Assembly

The line source assembly has a 27-cm long stainless steel tube (1.0-mm inside diameter). The tube is filled with radioactivity and both ends are sealed using specially designed caps equipped with small O-rings. The line source is similar to the line sources used in a commercially available PET-NEMA phantom (Data Spectrum Corp., Hillsborough, NC). For the collimated TCT studies presented here, the line source was typically filled with about 1110 to 7030 MBq (30–190 mCi) of ^{99m}Tc. After filling, the line source was placed on the central axis of the rotatable air-copper-lead attenuator assembly, which has accurately machined recesses matching the outside diameter of the line source sealing caps. Design of the rotatable air-copper-lead attenuator assembly allows the source to be easily and quickly removed for filling or replacement with another line source containing a different radionuclide. A photograph of the rotatable air-copper-lead attenuator assembly is shown in Figure 2.

The two main purposes of the rotatable air-copper-lead attenuators are: (1) to provide a means to position (and remove) selected gamma ray attenuators between the line source and the object being scanned; and (2) to provide a shielded enclosure for the line source (except in the direction of the object being scanned when the air or copper attenuator is positioned between the line source and the object).

The critical component of the rotatable air-copper-lead attenuator assembly is the rotating slotted cylinder. This slotted copper cylinder is mounted between two radial bearings and has six

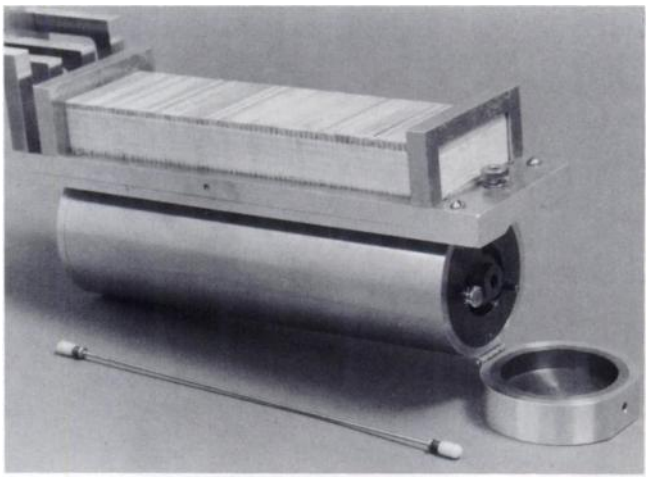

FIGURE 2. Photograph of prototype FB-TCT rotatable air-copper-lead assembly. The line source (shown in front of the assembly) is mounted along central axis of the rotatable air-copper-lead assembly.

annular sectors (Fig. 1). Four sectors (50 degrees each) are made of copper having different thicknesses. One sector (50 degrees) is made of lead laminated to the copper supporting cylinder (Fig. 1) and the remaining sector (110 degrees) is the open slot. The four copper sectors attenuate 140 keV gamma rays by factors of about 2, 4, 8 and 16. These attenuators are used to decrease the line source intensity to simplify the acquisition of reference FB image (i.e., data acquired when the patient is not present). Use of attenuators reduces the effects of system deadtime and pileup that may degrade the acquisition of the reference image. The lead sector attenuates the line source by a factor of more than 4 million.

During acquisition of FB-TCT projectional data, the rotatable air-copper-lead attenuator assembly was positioned with the open slot between the line source and the patient. During acquisition of SPECT emission data, the rotatable air-copper-lead attenuator assembly was positioned with the lead attenuator between the line source and the patient. For most studies presented here, the reference image was obtained shortly after actual FB-TCT acquisition using the copper attenuator that attenuates 140 keV gamma rays by a factor of 4. Generally, counting rates for the FB-TCT scans were similar to counting rates for the reference scan.

MultiSlat Collimator for Source

The major purposes of the multislat collimator are: (1) to eliminate gamma rays that have been emitted in directions inappropriate for FB-TCT acquisition; (2) to reduce radiation dose to the patient; and (3) to reduce the number of patient-scattered photons that are detected. The multislat collimator has 0.25-mm thick lead foils that have been glued to 1-mm thick spacers made of Rohacell (Rohm Tech, Inc., Malden, MA), which is a special gamma ray transparent foam having highly uniform thickness. The multislat collimator has alternating layers of lead foil plates and Rohacell spacer plates. The planes of the lead foil plates and the Rohacell spacer plates are perpendicular to the axis of rotation. Each Rohacell spacer plate has the same height and thickness as the lead foil plates with a height of 4.5 cm and a width of 7.6 cm.

Fan-Beam Collimator for Opposing Scintillation Camera

The two main purposes of the fan-beam collimator (Nuclear Fields, Inc., Des Plaines, IL) mounted on the scintillation camera opposite the line source, are: (1) to reduce the detection of patient scattered gamma rays; and (2) to provide collimation for transmission and emission gamma rays. The fan-beam collimator has a focal length of 114 cm (to crystal side) and hexagonal holes. The TCT fan-beam collimator has a geometric sensitivity of 270 (counts/sec)/MBq (10 (counts/sec)/μCi) at 10 cm from the collimator surface and a geometric resolution (FWHM) of 10 mm at 10 cm from the collimator surface.

A low-energy, ultra-resolution (LEUR) parallel-hole collimator was used with the collimated curved slab source to obtain parallel-beam TCT data. This collimator also was used to acquire the SPECT data. The LEUR parallel-hole collimator has a geometric sensitivity of 81 (counts/sec)/MBq (3 (counts/sec)/μCi) and a geometric resolution (FWHM) of 6.2 mm at 10 cm from the collimator surface.

Phantoms

To evaluate total system resolution, a plastic rod phantom was scanned using the transmission line source assembly and curved slab source. The plastic "cold" rod phantom (Deluxe Model 5000, Data Spectrum Corp., Hillsborough, NC) has a circular cylinder (22 cm outside diameter) containing six sets of plastic (methylmethacrylate) rods having different diameters. The rod diameters are 4.8, 6.4, 7.9, 9.5, 11.1 and 12.7 mm. The center-to-center spacing between the rods is equal to twice the diameter of the rods. The rods are 8.8 cm long and are arranged in six "pie-shaped" sectors within the cylindrical phantom, which is filled with air. The plastic cylinder has a wall thickness of approximately 3 mm. The phantom is placed in an aluminum cradle (3-mm thick wall) during the acquisition of TCT data.

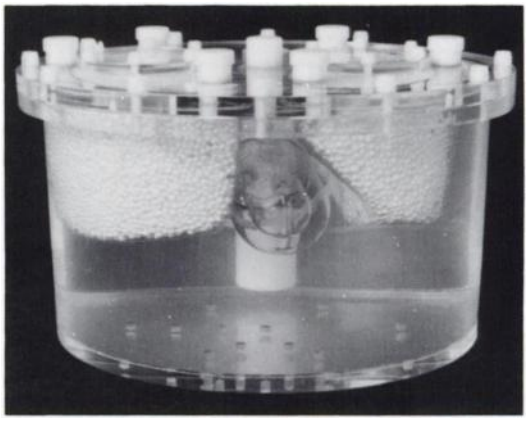

FIGURE 3. Photograph of the smaller thorax phantom consisting of an elliptical cylinder with anthropomorphic heart, lung and spine inserts. The larger thorax phantom was constructed by placing water-filled bags around the periphery of this phantom to increase overall dimensions and simulate breast tissue.

An anthropomorphic thorax phantom (Data Spectrum Corp., Hillsborough, NC) was also used to evaluate the transmission CT system. The phantom is shown in Figure 3 and has an elliptical cylinder (32 cm × 23 cm) containing two lung inserts, a Teflon spine and a cardiac insert. The Teflon spine consists of a solid cylinder 3.8 cm in diameter by 16.5 cm in length. The two lung inserts contain styrofoam beads and are filled with water to simulate the density of lung tissue. For the studies presented here, water and bead volumes were adjusted for each lung chamber to obtain a density of approximately 0.3 gm/cm^3. The cardiac insert contains a ventricle chamber and a myocardial chamber. Each chamber may be filled separately with water containing activity. This phantom is referred to as the "small" thorax phantom. To simulate a larger patient and to investigate the effects of truncation, we added water-filled bags around the periphery of this phantom to increase its dimensions to approximately 38 cm × 26 cm. We also added water-filled bags (500-ml) to simulate breast tissue. This phantom is referred to as the "large" thorax phantom. For this investigation we filled the myocardial chamber with activity.

Patient Studies

Two female patients who were scheduled to have myocardial SPECT studies were scanned using the TCT system prior to their myocardial studies. Informed consent was obtained prior to the study using a protocol approved by the Institutional Review Board of the medical center. The first patient weighed 140 lb and was 5 ft 6 in. tall. There was little truncation of the transmission projection for this patient study. The second patient weighed 114 lb and was 4 ft 11 in. tall. The transmission data were severely truncated for the second patient study. For the first patient, the transmission data were acquired prior to injection of the SPECT radiopharmaceutical. For the second patient, FB-TCT data were

acquired after injection of ^{201}Tl and immediately prior to the SPECT study.

TCT Data Acquisition

The TCT and SPECT data were transferred using our departmental Ethernet network to a Stellar GS1000 (Stardust Computers, Inc., Newton, MA) and Sun Sparcstation-2 computers (Sun Microsystems, Inc., Mountain View, CA) for image reconstruction and data analysis. The following TCT and SPECT acquisitions were obtained:

1. Parallel-beam and FB-TCT scans of the cold rod phantom.
2. A parallel-beam TCT scan of the small thorax phantom.
3. An uncollimated 63-cm focal length (measured from the crystal surface) FB-TCT scan of the small thorax phantom. The 63-cm focal length refers to the distance of the line source to the crystal surface of the opposed scintillation camera, which did not have a collimator mounted on it. In this case, the multislice fan-beam geometry is determined by the line source and the multislat collimator placed directly beneath the line source.
4. Two (120 and 750 sec) FB-TCT scans of the small thorax phantom without ^{201}Tl radioactivity in the myocardial chamber.
5. A FB-TCT scans of the small thorax phantom with and without ^{201}Tl radioactivity in the myocardial chamber.
6. A FB-TCT scan of the large thorax phantom with ^{201}Tl radioactivity in the myocardial chamber.
7. A parallel-beam SPECT scan of the large thorax phantom with ^{201}Tl radioactivity in the myocardial chamber.
8. FB-TCT scans of the first female patient with no radioactivity in the myocardial chamber.
9. FB-TCT scans of the second female patient with ^{201}Tl radioactivity in the myocardial chamber.
10. Parallel-beam SPECT scans of second female patient with ^{201}Tl radioactivity in the myocardial chamber.

Typically, data were acquired using an acquisition matrix size of 128 × 128 and 3-degree angular sampling with step-and-shoot gantry motion through a complete 360-degree angular range. A few scans were also acquired using continuous gantry rotation. A 15% centered energy window (130 keV ≤ Eγ ≤ 151 keV) was used for the TCT acquisitions. For the ^{201}Tl SPECT scan, the energy window ranged from approximately 60 to 80 keV. Additional acquisition parameters are presented in Table 1. Filtered backprojection algorithms were used to reconstruct the TCT and SPECT images.

The small-thorax phantom was scanned both with the fan-beam TCT geometry and with a parallel-beam TCT geometry, which consisted of a collimated curved slab source and a high-resolution, parallel-hole collimator (*5,9*) mounted directly under the slab source. For the parallel-beam TCT acquisition, use of a collimated curved slab source resulted in a 40-cm field-of-view (FOV) and adequate clearance to scan the thorax phantom. The curved transmission source (containing about 220 MBq/axial cm (5.9 mCi/axial cm) of ^{99m}Tc) was mounted between two scintillation cameras of the triple-head SPECT system. The LEUR parallel-hole collimator was placed on the third scintillation camera.

To show effects of truncated projections on TCT image quality, the small thorax phantom was scanned with the line source positioned at 63 cm from the crystal surface of the opposing scintillation camera, which did not have a collimator (scan no. 3, listed above). In this case, the multislice fan-beam geometry is determined by the line source and the multislat collimator, which is placed directly beneath the line source.

The 114-cm focal length fan-beam collimator was then placed on the scintillation camera and the line source was positioned at 110 cm from the crystal surface. Before mounting the line source, we machined a rectangular opening in the side cover panels of the triple-camera system. These openings provide adequate clearance to mount the line source at 110 cm. Further modification of the gantry would be necessary to position the line source exactly at the 114-cm focal line of the fan-beam collimator. Although the 110-cm location is not optimal, we found that gamma ray intensity was adequate, even at the edges of the FOV.

The ^{99m}Tc activity in the line source ranged between 30 and 60 MBq/axial cm (0.8 and 1.6 mCi/axial cm). Several FB-TCT scans of the small and large thorax phantoms were acquired. For two scans (120 and 750 sec total scan times), no ^{201}Tl activity was placed in the myocardial chamber of the thorax phantoms. For two scans of the thorax phantoms (750 sec total scan time), 5.4 MBq (145 μCi) were placed in the myocardial chamber.

The rotatable air-copper-lead attenuator assembly was then closed (i.e., the lead attenuator was placed between the line source and the thorax phantom) and a ^{201}Tl SPECT scan was performed (360-degree acquisition and a total scan time equal to 1440 sec). Only the two cameras having ultra-high resolution (LEUR), parallel-hole collimators were used for the SPECT acquisition. However, we used the data acquired with the fan-beam collimator to estimate amount of spillover of ^{201}Tl photons into the ^{99m}Tc window which was used for the TCT scans. The first eight projectional views were quantitatively evaluated by determining the counting rate within regions of interests (ROIs) that completely encompassed the projection of the heart on the scintillation camera equipped with the fan-beam collimator. These ROI data were used to estimate the number of ^{201}Tl photons emitted from the heart that were detected within the ^{99m}Tc energy window. These data were compared with similar ROI data obtained from the FB-TCT scans (with no ^{201}Tl activity in the heart). These latter ROI data were used to determine the number of ^{99m}Tc photons (from the line source) that were detected within the ^{99m}Tc energy windows. This analysis indicated that the ^{201}Tl spillover was only about 1% of the true ^{99m}Tc photons emitted by the transmission line source. Since only a very small number of ^{201}Tl photons were detected in the ^{99m}Tc energy window, no attempt was made to subtract these ^{201}Tl photons prior to reconstructing the ^{99m}Tc TCT images.

After closing the rotatable air-copper-lead attenuator assembly, we observed that a few photons emitted from the rotatable air-copper-lead attenuator assembly still reached the opposing scintillation camera. We assumed that these photons were scattered by the two copper sectors that were adjacent to the 50-degree lead sector. Thus, for the SPECT acquisition, these scattered photons were eliminated by placing a 6.4-mm thick lead sheet under the multislat collimator. To eliminate these photons in the future, we have redesigned the rotatable air-copper-lead attenuator assembly by doing away with one copper sector and increasing the angular extent of the remaining lead and copper sectors from 50 degrees to 62.5 degrees.

Image Reconstruction

The measured transmission data were converted to line integrals of linear attenuation by taking the natural logarithm of the ratio of the incident reference image to the measured TCT projectional data. Before taking the logarithm, the reference image

TABLE 1
TCT Data Acquisition Parameters

Scan type	Source type used	Line (slab) source activity (MBq/axial cm)	Line source to crystal distance (cm)	Radius of rotation* (cm)	Collimator type	Total acquisition interval (sec)	^{201}Tl myocardium activity (MBq)
Parallel-beam TCT; cold rods	Curved slab	247	110	26	Parallel-hole (LEUR)	2200	None
Fan-beam TCT; cold rods	Line	62	110	25	Fan-beam	2120	None
Parallel-beam TCT; thorax	Curved slab	220	N/A†	25	Parallel-hole (LEUR)	750	None
Fan-beam TCT; small thorax	Line	3	63	25	Fan-beam	750	None
Fan-beam TCT; small thorax	Line	46	110	25	Fan-beam	120	None
Fan-beam TCT; small thorax	Line	46	110	25	Fan-beam	750	None
Fan-beam TCT; small thorax	Line	32	110	25	Fan-beam	775	5.4‡
Fan-beam TCT; large thorax	Line	88	112	28	Fan-beam	720	4.8‡
Fan-beam TCT; first patient	Line	118	109	25	Fan-beam	720	0
Fan-beam TCT; second patient	Line	260	108	28	Fan-beam	900	148§
Parallel-beam SPECT; large thorax	N/A	N/A	N/A	28	Parallel-hole (LEUR)	1200	4.8‡
Parallel-beam SPECT; second patient	N/A	N/A	N/A	28	Parallel-hole (LEUR)	1200	148§

*To crystal side.
†Not applicable.
‡In heart wall chamber.
§Injected activity at time of scan.

was scaled to account for differences in the acquisition procedure between it and the TCT data. The scaling accounted for differences in acquisition time, deadtime, radioactive decay and the effect of attenuation of the reference image by the copper attenuator.

TCT and SPECT data (360-degree data acquisitions) were reconstructed using filtered backprojection algorithms. A 128 × 128 (3.6-mm pixel size) matrix was used. Generalized Hann filters having cut-off frequencies between 0.5 cycle/cm and 1.0 cycle/cm were used. Typically, lower cut-off frequencies were used with lower count density TCT data, while higher cut-off frequencies were used with higher count density TCT data. A ramp filter was used for the TCT reconstructed images of the cold rod phantom.

Adjacent reconstructed slices were added to reduce image noise. Generally, the displayed slice thickness was equal to 11 mm for TCT images of the thorax, and 7 cm for the TCT images of the cold rod phantom.

A similar reconstruction protocol was used for the SPECT data of the thorax phantom. However, attenuation compensation was done using a single iteration Chang algorithm (*16*) that was modified to incorporate a nonuniform attenuation map (*12,13*). Three sets of SPECT images were reconstructed with: (1) no attenuation compensation; (2) uniform attenuation compensation using an assumed linear attenuation coefficient equal to 0.15 cm^{-1}; and (3) attenuation compensation using the nonuniform map measured with FB-TCT. The TCT-measured attenuation values measured with the FB-TCT scan were used to correct the ^{201}Tl SPECT data. The measured attenuation values were not scaled to account for the energy difference between the transmission and emission sources. To account for scatter in the ^{201}Tl emission data, no scaling was performed. Although reconstructed attenuation values using the ^{99m}Tc line source were inappropriately small for narrow-beam linear attenuation coefficients at the ^{201}Tl energy, fortuitously, they were reasonable for broad-beam coefficients at this energy (broad-beam implying the detection of scatter events). A similar approach to account for scatter with ^{99m}Tc was used previously (*17*).

Determination of Linear Attenuation Coefficients

To find the values for the linear attenuation coefficients, ROIs were drawn on reconstructed TCT images of the thorax phantom. We used the software program SPECTER to display images and obtain ROI values. Several ROIs were used to sample lung, soft tissue and spinal regions. Typically, each ROI contained about 50 pixels, although smaller ROIs were used for the spinal region. ROI values were determined with, and without ^{201}Tl in the myocardial chamber. ROI results were also obtained from TCT reconstructed images using reference images that were measured with and without ("in-air") a copper attenuator.

The TCT-measured attenuation coefficients were compared

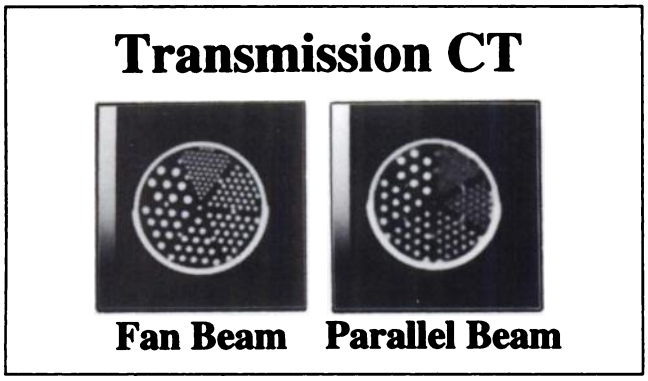

FIGURE 4. Fan-beam and parallel-beam TCT reconstructed images of the cold plastic rod phantom. The FB-TCT image shows improved image quality compared with the parallel-beam TCT image.

with narrow-beam values. These narrow-beam coefficients were measured using a well-collimated (narrow-beam) ^{99m}Tc transmission source and known thicknesses of water, lung and spinal material. A 15-mm thick Pb sheet with a 7-mm diameter hole drilled through it was placed on the collimator surface. A second 8-mm thick Pb disk with a 2-mm diameter hole drilled through it was placed 13 cm above the surface of the first Pb sheet. A third 13-mm thick Pb disk with a 2-mm diameter hole drilled through it was placed 19 mm above the surface of the second disk. A 925-MBq (25 mCi) ^{99m}Tc source (approximately 4 mm in diameter) was positioned directly above the hole in the third disk. The centers of all three holes were positioned to fall on a line that was perpendicular to the collimator surface. A scintillation camera was used to detect the transmitted gamma rays, and a low counting rate (less than 1 kcounts/sec) was used to minimize dead-time losses. The energy window ranged from 130 keV to 150 keV. Samples of water or "soft tissue" (7.8 cm thick), Teflon or "bone tissue" (8.8 cm thick) and water-filled styrofoam beads "lung tissue" (13.1 cm thick) were placed between the first and second Pb disks. A 9 cm × 9 cm ROI was used to determine the transmitted source intensity. The "in air" reference source intensity was also measured with only air between the first and second Pb disk. Background counting rates were measured and were found to be less than 0.3% of the counting rates measured with the source present. Ten independent measurements were made for each material. These measurements were used to determine the average narrow-beam linear attenuation coefficients and corresponding standard deviations.

RESULTS

The parallel-beam and fan-beam TCT reconstructed images of the cold rod phantom are shown in Figure 4. These images were reconstructed using a fan-beam filtered backprojection algorithm with a ramp filter. The thin aluminum cradle (3 mm thick) used to support the phantom is seen surrounding the lower portion of the cylindrical phantom. Plastic support rods (6.4 mm diameter) are seen in the center of the image and in regions between the six sectors. This image shows that high-resolution TCT images can be obtained using the transmission line source assembly. All six sectors of the cold rod insert are clearly visualized in the FB-TCT images, but only five sectors are visualized in the parallel-beam TCT image.

Three different TCT scans of the thorax phantom are presented in Figure 5. The transmission projections were reconstructed using an image matrix size of 128 × 128 × 128. The same generalized Hann filter having a cut-off frequency equal to 1.4 cycles/cm was used to reconstruct the parallel-beam, the short focal length fan-beam and the long focal length fan-beam data. The same fan-beam reconstruction algorithm was used to reconstruct all three data sets. The parallel-beam TCT image was reconstructed by setting the focal length equal to 9999 cm in the fan-beam reconstruction program.

The short (63 cm) focal length fan-beam scan has large artifacts caused by truncated projections. These artifacts have been nearly eliminated in the TCT image obtained using the longer (110 cm) focal length scan. The 110-cm FB-TCT reconstructed image is similar in appearance to the parallel-beam TCT image; however, the longer focal length FB-TCT image shows improved spatial resolution and less noise compared with the parallel-beam TCT image. Horizontal profiles drawn through the central portion of the FB-TCT images and the parallel-beam TCT image are shown in the lower portion of Figure 5. The reduction in noise in the FB-TCT image results from the increased number of transmission photons detected with the line source fan-beam collimator geometry compared with the number of photons detected with the slab source parallel-hole collimator geometry. The heart insert is not visualized in these TCT reconstructed images since the ventricle and myocardial chambers are filled with water, which has the same density as the surrounding water tissue. The Teflon spine is clearly visualized.

The FB-TCT reconstructed images obtained using total acquisition time intervals of 120 and 750 sec are shown in Figure 6. The cut-off frequency of the reconstruction filter

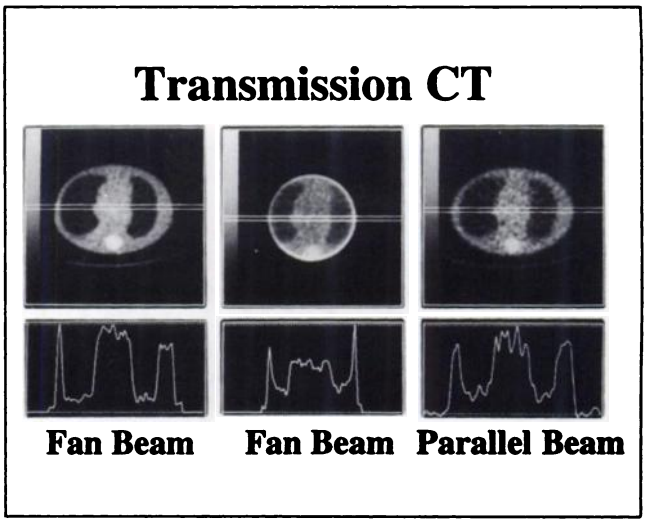

FIGURE 5. Fan-beam and parallel-beam TCT reconstructed images of the thorax phantom. The 63-cm FB-TCT reconstructed image (center) demonstrates substantial truncation artifacts. The 110-cm FB-TCT reconstructed image (left) has almost no truncation artifacts and shows improved image quality compared with the parallel-beam TCT reconstructed image (right).

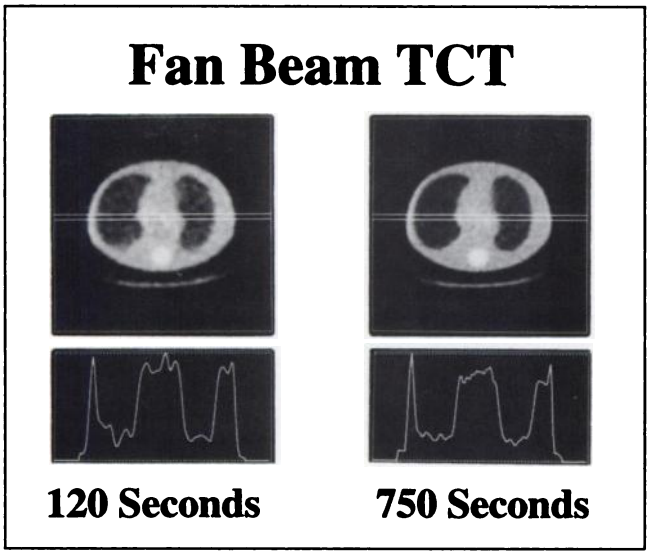

FIGURE 6. FB-TCT reconstructed images acquired with two different acquisition time intervals.

was lower for the 120-sec image than the cut-off frequency for the 750-sec image. With the same cut-off frequency, the 120-sec image would have increased noise, but it still may provide an acceptable attenuation map for SPECT nonuniform attenuation.

Fan-beam-TCT reconstructed images of the thorax phantom acquired with and without ^{201}Tl activity in the myocardial chamber are shown in Figure 7. The ratio of ^{201}Tl photons that were detected in the ^{99m}Tc energy window to the 140 keV photons that were detected in this energy window was approximately 87:1. This ratio was determined from the projection data using appropriately placed ROIs. Only a very small number of ^{201}Tl photons were detected in the ^{99m}Tc energy window, compared with the number of ^{99m}Tc photons detected in this window. Because of this very small number, a subtraction compensation was not required. The two images shown in Figure 7

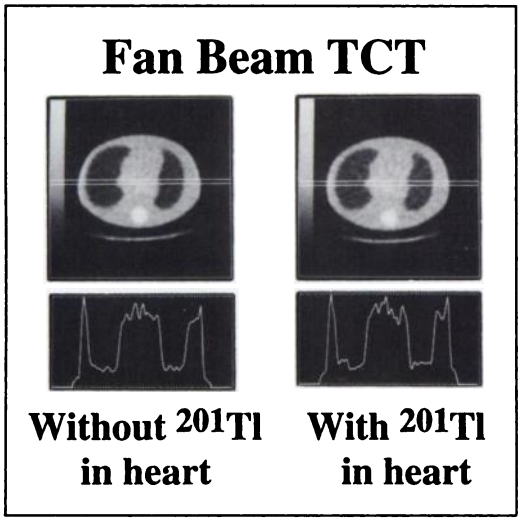

FIGURE 7. FB-TCT reconstructed images of the thorax phantom with, and without, ^{201}Tl activity in the myocardial chamber. The FB-TCT images are very similar.

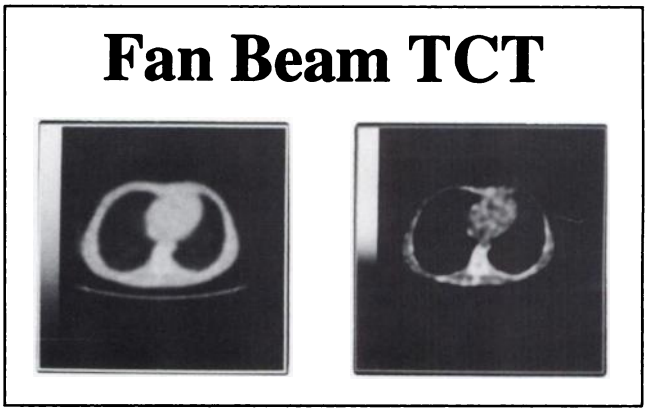

FIGURE 8. Fan-beam TCT reconstructed transaxial slices of the first female patient. The ribs, vertebra and spinal column are visualized in the windowed display shown on the right.

are very similar. Since there was less line source activity in the image acquired with ^{201}Tl activity than in the image acquired without ^{201}Tl activity (Table 1), the noise level is somewhat higher for the image with ^{201}Tl activity present. Horizontal profiles drawn through the central region of images are shown at the bottom of Figure 7.

A FB-TCT image of the first female patient is shown in Figure 8. For the image shown on the right, the data were windowed to increase the displayed image contrast. The ribs, vertebra and spinal column are more clearly visualized with the windowed display.

The effect of nonuniform attenuation on SPECT cardiac imaging was evaluated with the larger thorax phantom and with the second patient scans. These data are shown in Figures 9 and 10, respectively. The FB-TCT images shown in the upper right corner of these figures demonstrate the effect of truncation. The upper row of profiles has been normalized independently. The lower row of profiles has been normalized to the peak value obtained when a uniform attenuation map (i.e., constant linear attenuation co-

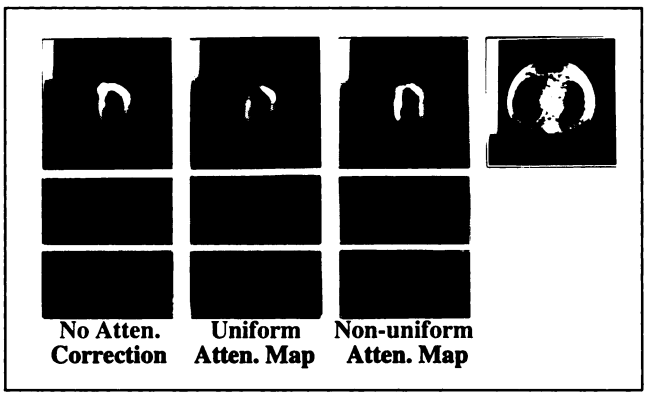

FIGURE 9. Fan-beam reconstructed TCT transaxial slice (upper right) and horizontal long axis SPECT heart slices of the larger thorax phantom. Effect of transmission data truncation is visualized in the TCT image. Upper profiles have been normalized independently. Lower profiles have been normalized to peak value of profile obtained using a uniform attenuation map. The SPECT image reconstructed using a nonuniform attenuation map has fewer artifacts and less distortion compared with the other two reconstructions.

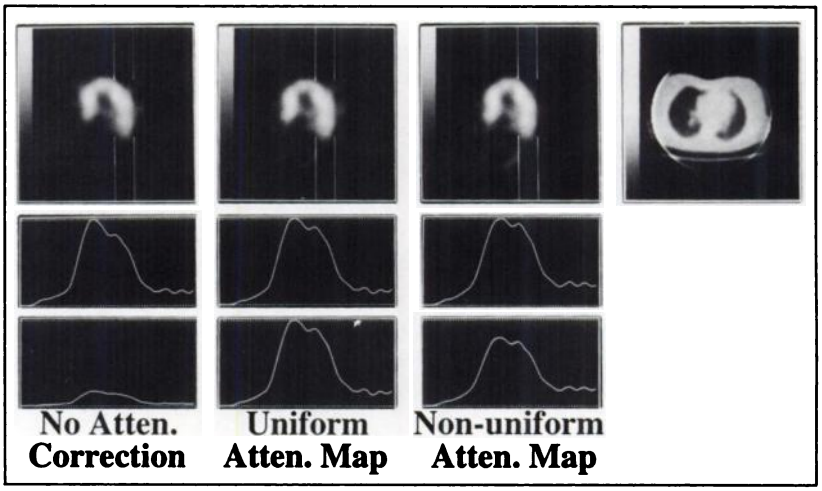

FIGURE 10. Fan-beam reconstructed TCT transaxial slice (upper right) and horizontal long axis SPECT heart slices of second female patient. Effect of transmission data truncation is visualized in the TCT image. Upper profiles have been normalized independently. Lower profiles have been normalized to peak value of profile obtained using a uniform attenuation map.

efficient) was used to compensate for attenuation. The profiles were determined by summing the counts within the vertical markers. The left-to-right direction in the profiles corresponds to the top-to-bottom direction in the images. The lower row of profiles more realistically demonstrates the quantitative effects of the three different reconstruction methods. The horizontal long-axis SPECT images reconstructed using the nonuniform attenuation map are qualitatively and quantitatively improved compared with the other two images. In this initial evaluation, no attempt was made to compensate for truncation of transmission data. Without attenuation compensation, the reconstructed pixel values are markedly reduced compared with the values observed in the other two images. Use of a uniform attenuation map results in an overcompensation. The general shape of the long axis slice through the heart phantom is distorted in the absence of nonuniform attenuation compensation.

Measured linear attenuation coefficients are shown in Table 2. The measured values obtained with the parallel-beam and fan-beam TCT reconstructed images agree well with the values obtained using narrow-beam transmission measurements. The linear attenuation coefficients measured with and without ^{201}Tl in the myocardial chamber are very similar. Also, the values measured using the air reference image agree well with the coefficients measured using the reference image obtained with the copper attenuator positioned between the line source and the scintillation camera. Some of the TCT-measured values appear slightly lower than the narrow-beam values, particularly the values measured in the spine region. It is possible that the slightly lower values measured with parallel-beam and fan-beam TCT are the result of Compton scatter detected within the TCT energy window.

DISCUSSION

Results of the phantom and patient studies show that fast, sequential TCT scanning using a line source and rotatable air-copper-lead attenuator assembly provides improved image quality compared with parallel-beam TCT. Fan-beam TCT has several practical advantages compared with parallel-beam TCT, particularly when used with triple-camera SPECT systems. For parallel-beam TCT, the

TABLE 2
Measured Attenuation Coefficients

Method	Linear attenuation coefficient (cm^{-1})		
	Lung	Tissue	Spine
Narrow-beam transmission	0.049 ± 0.003	0.153 ± 0.002	0.291 ± 0.005
Parallel-beam TCT	0.050 ± 0.002*	0.152 ± 0.006	0.279 ± 0.005
Fan-beam TCT without ^{201}Tl (air reference beam)	0.044 ± 0.003	0.147 ± 0.005	0.272 ± 0.004
Fan-beam TCT without ^{201}Tl (copper attenuator)	0.046 ± 0.004	0.149 ± 0.006	0.274 ± 0.005
Fan-beam TCT with ^{201}Tl (copper attenuator)	0.044 ± 0.003	0.147 ± 0.005	0.268 ± 0.007

*Mean ± s.d.

curved slab source must be mounted between two adjacent cameras; thus, these cameras cannot be used for simultaneous SPECT acquisition. Fast sequential TCT acquisition is impractical with parallel-beam TCT. The curved collimated slab source must be mounted on the two uncollimated cameras to provide adequate patient clearance. The source must be manually removed and the collimators replaced before the SPECT study. The collimated slab source must be filled with a large amount of radioactivity to obtain adequate count densities within reasonable scan times. Therefore, radiation exposure to technical support personnel is increased. Also, since the slab source is large, it is more difficult to shield when it is not being used.

Fan-beam TCT using a line source and a rotatable air-copper-lead attenuator assembly overcomes many of these practical problems. For example, since the assembly is not mounted on or in front of a gamma camera, there is no interference with the acquisition of SPECT data, and the collimators do not have to be replaced before the SPECT scan. The lead and copper attenuators can be quickly and easily positioned. Line sources filled with different radioisotopes may be interchanged conveniently. The shielded rotatable air-copper-lead attenuator assembly provides a useful storage location for the source when it is not being used. Thus, radiation exposure to the technical support personnel is minimized.

Some of these advantages are also possible with cone-beam TCT (*6*) using a point source. Only a small amount of radioactivity is required with cone-beam TCT since an uncollimated point source is used with this acquisition geometry. However, cone-beam TCT has inadequate axial sampling which may produce artifacts in the reconstructed image. Fan-beam TCT has adequate sampling in the axial direction; thus, there are no artifacts produced in the reconstructed image for object locations away from the central plane. Both fan-beam and cone-beam TCT may result in truncated projections when large patients are scanned. However, Tung et al. (*7*) have found that though the TCT reconstructed image is distorted for regions outside the field-of-view, the attenuation factors are fairly accurate.

Tung et al. (*7*) used an iterative reconstruction algorithm and a somewhat short 65-cm focal-length collimator. We use a much longer focal length fan-beam collimator by moving the detectors away during the fast sequential TCT acquisition. With our FB-TCT geometry, the maximum useful field-of-view is about 32 cm. Therefore, we observed very little truncation of transmission projection data when imaging the smaller thorax phantom and the smaller patient. For the larger thorax phantom and the larger patient, transmission data were more severely truncated and artifacts were observed in the TCT images. Further research is required to determine whether methods can be developed to minimize the important problems associated with truncated projections. It may be possible to extrapolate the truncated data using body contour information. This information may be available from the parallel-beam SPECT acquisition using a lower energy scatter window. The resulting TCT image may then be adequate for SPECT attenuation compensation. Furthermore, it is possible to use iterative reconstruction algorithms to reduce truncation artifacts (*7,18*), but these algorithms have a larger computational burden compared with filtered backprojection algorithms. In the future, triple-camera SPECT systems that use larger field-of-view scintillation cameras may become available. Truncation of the projections would be less severe with these systems and it is anticipated that the quantitative accuracy of the SPECT reconstruction would be improved.

The effect of nonuniform attenuation on SPECT myocardial imaging depends on many factors including the size and shape of the patient and the size, shape and location of the myocardial defect. The acquisition protocol (e.g., 360 degrees versus 180 degrees) and the reconstruction algorithm can also influence the quantitative accuracy of the SPECT image. Results presented here apply only to specific source geometries used in this study. Further research is required to determine if these techniques are appropriate for other source geometries.

Use of nonuniform attenuation data quantitatively improved the SPECT scan of the myocardial chamber containing ^{201}Tl. A study based on receiver operator characteristics (ROC) would help to decide the usefulness of nonuniform attenuation in cardiac lesion detection. We are planning to perform this ROC study soon.

The minimum scan time for the TCT acquisition is determined mainly by counting rate and deadtime considerations. With a line source containing about 45 MBq/axial cm (1.2 mCi/axial cm) of ^{99m}Tc and with the 1-mm thick Rohacell®-lead multislat collimator, the counting rate was about 20 kcounts/sec when scanning the thorax phantom. When the phantom was removed, the counting rate was about 25 kcounts/sec with the use of the copper attenuator and about 100 kcounts/sec without the attenuator. Since it should be possible to acquire TCT data at counting rates (per head) of at least 100 kcounts/sec, adequate count densities for a single line source should be possible with scan times of about 2 min. Even shorter scan times would be possible if three line sources were used with all three heads of a triple-camera system or if camera deadtimes were reduced.

The specific activity for the ^{99m}Tc line source used in this study was about 2200 MBq/ml (60 mCi/ml). This activity was obtained by using 10 ml of saline to elute the ^{99}Mo generator. It is possible to obtain a specific activity of about 24,000 MBq/ml (650 mCi/ml) by using a smaller volume of 2–3 ml to elute the generator. Since the line source has a volume less than 0.5 ml, the higher specific activity would greatly increase the transmission counting rates. Therefore, either the scanning time could be markedly decreased or the signal-to-noise ratio of the TCT reconstructed image could be improved. Of course, the scintillation camera and associated electronic circuitry must be capable of processing the high counting rates.

For the results presented here, the fan-beam collimator

was used only for the acquisition of TCT data but it could potentially be used to acquire improved SPECT data. We have previously shown that converging-beam SPECT data can be combined with parallel SPECT data (*18*). Thus, SPECT data obtained using two fan-beam collimators could be combined with SPECT data acquired with the parallel-hole collimator mounted on the other scintillation camera of the triple-camera system. This method would avoid problems associated with truncation of the SPECT projections. Alternatively, all three scintillation cameras could be equipped with fan-beam collimators. This acquisition approach has the potential to improve the quality of both the SPECT and the TCT scans.

In this initial investigation, we made no effort to optimize the design of the multislat and fan-beam collimators. Optimal sensitivity and resolution characteristics for these collimators should be determined. Recently, Cao and Tsui described an analysis of precollimation and postcollimation for parallel-beam TCT (*19*). A similar analysis would be useful for fan-beam TCT.

CONCLUSIONS

We describe a method to quickly and easily acquire the TCT data needed to determine nonuniform attenuation maps for SPECT attenuation compensation. The method uses a line source and a rotatable air-copper-lead attenuator assembly and minimizes problems associated with crosstalk between the transmission and emission data. The nonuniform attenuation maps are used to compensate SPECT phantom and patient scans with ^{201}Tl activity in the myocardial chamber. Qualitatively and quantitatively, the SPECT images are improved using the nonuniform attenuation data. With our present triple-camera system, truncation of the transmission data was observed for the larger thorax phantom and the larger patient. Results indicate that approaches should be considered to minimize effects of truncation on SPECT reconstruction. One approach would be to use a single larger field-of-view camera. A second potential approach would be to use SPECT scatter-window data acquired with parallel-hole collimators. Further research is required to decide the importance of nonuniform attenuation compensation on SPECT lesion detection in cardiac ^{201}Tl studies. These results show the feasibility of using fast, sequential transmission scans of a line source mounted within a rotatable air-copper-lead attenuator assembly to obtain accurate attenuation maps.

ACKNOWLEDGMENTS

The authors thank Ms. Gail Steinke for her excellent secretarial support in preparing this manuscript; Mr. D. York (Precise Corp., Caryville, TN) for freely providing us the lead foil for the multislat collimator; Mr. A. van Mullekom (Nuclear Fields, Inc., Des Plaines, IL) for help with the design of the fan-beam collimator; and Mrs. N. Jaszczak (Data Spectrum Corp., Hillsborough, NC) for allowing us to use the cold rod and thorax phantoms. This investigation was supported in part by Public Health Service grant number CA33541 awarded by the National Cancer Institute and by Department of Energy Grant DE-FG05-89ER60894. Partial support for the research triple-camera SPECT system was provided by a Public Health Service instrumentation grant S10-RR04176 and by a Department of Energy instrumentation grant DE-FG05-91ER75577. We acknowledge use of the software package "SPECTER" developed in our laboratory by T. Turkington. We thank him for his efforts in expanding the capabilities of SPECTER to suit our specific requirements. Dr. Jaszczak is a consultant to, and an officer of Data Spectrum Corporation. Selected aspects of this research were presented at the 1992 IEEE Medical Imaging Conference (Orlando, October 1992) and a short description appeared in the nonarchived conference record for that meeting.

REFERENCES

1. Jaszczak RJ, Chang L-T, Stein NA, Moore FE. Whole-body single photon emission computed tomography using dual, large-field-of-view scintillation cameras. *Phys Med Biol* 1979;24:1123–1143.
2. Greer KL, Harris CC, Jaszczak RJ, et al. Transmission computed tomography data acquisition with a SPECT system. *J Nucl Med Tech* 1987;15:53–56.
3. Bailey DL, Hutton BF, Walker PJ. Improved SPECT using simultaneous emission and transmission tomography. *J Nucl Med* 1987;28:844–851.
4. Tsui BMW, Gullberg GT, Edgerton ER, et al. Correction of nonuniform attenuation in cardiac SPECT imaging. *J Nucl Med* 1989;30:497–507.
5. Gilland DR, Jaszczak RJ, Coleman RE. Effects of nonuniform attenuation compensation in SPECT using acquired transmission data [Abstract]. *J Nucl Med* 1991;32:1067.
6. Manglos SH, Bassano DA, Thomas FD. Cone beam transmission computed tomography for nonuniform attenuation compensation of SPECT images. *J Nucl Med* 1991;32:1813–1820.
7. Tung CH, Gullberg GT, Zeng GL, Christian PE, Datz FL, Morgan HT. Nonuniform attenuation correction using simultaneous transmission and emission converging tomography. *IEEE Trans Nucl Sci* 1992;39:1134–1143.
8. Bailey DL, Eberl S, Tan P, Meikle SR, Fulton RR, Hutton BF. Implementation of a scanning line source for attenuation correction with simultaneous emission/transmission SPECT [Abstract]. *J Nucl Med* 1992;33:901.
9. Gilland DR, Jaszczak RJ, Turkington TG, Greer KL, Coleman RE. Transmission data acquisition with a three-headed SPECT system [Abstract]. *J Nucl Med* 1992;33:901.
10. Malko JA, Van Heertum RL, Gullberg GT, Kowalsky WP. SPECT liver imaging using an iterative attenuation correction algorithm and an external flood source. *J Nucl Med* 1986;27:701–705.
11. Manglos SH, Jaszczak RJ, Floyd CE. Weighted backprojection implemented with a nonuniform attenuation map for improved SPECT quantification. *IEEE Trans Nucl Sci* 1988;NS-35:625–628.
12. Manglos SH, Jaszczak RJ, Floyd CE, Hahn LJ, Greer KL, Coleman RE. A quantitative comparison of attenuation-weighted backprojection with multiplicative and iterative postprocessing attenuation compensation in SPECT. *IEEE Trans Med Imag* 1988;7:127–134.
13. Gilland DR, Jaszczak RJ, Greer KL, Coleman RE. Quantitative SPECT reconstruction of iodine-123 data. *J Nucl Med* 1991;32:527–533.
14. Frey EC, Tsui BMW, Perry R. Simultaneous acquisition of emission and transmission data for improved thallium-201 cardiac SPECT using a technetium-99m transmission source. *J Nucl Med* 1992;33:2238–2245.
15. Galt JR, Cullom SJ, Garcia EV. SPECT quantification: a simplified method of attenuation and scatter correction for cardiac imaging. *J Nucl Med* 1992;33:2232–2237.
16. Chang L-T. A method for attenuation correction in radionuclide computed tomography. *IEEE Trans Nucl Sci* 1978;NS-25:638–643.
17. Manglos SH, Jaszczak RJ, Floyd CE, Hahn LJ, Greer KL, Coleman RE. Nonisotropic attenuation in SPECT: phantom tests of quantitative effects and compensation techniques. *J Nucl Med* 1987;28:1584–1591.
18. Jaszczak RJ, Li J, Wang H, Coleman RE. Three dimensional SPECT reconstruction of combined cone beam and parallel beam data. *Phys Med Biol* 1992;37:535–548.
19. Cao Z-J, Tsui BMW. Performance characteristics of transmission imaging using a uniform sheet source and parallel-hole collimation. *Med Phys* 1992;19:1205–1212.